Journal of Analytical and Applied Pyrolysis 168 (2022) 105724

Contents lists available at ScienceDirect

Journal of Analytical and Applied Pyrolysis

journal homepage: www.elsevier.com/locate/jaap

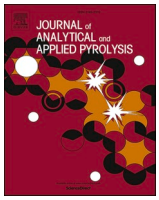

Effect of heating rate and H_3PO_4 as catalyst on the pyrolysis of agricultural residues

Behnam Hosseinzaei [a], Mohammad Jafar Hadianfard [a,*], Ramiro Ruiz-Rosas [b], Juana M. Rosas [b], José Rodríguez-Mirasol [b,*], Tomás Cordero [b]

[a] Department of Materials Science and Engineering, School of Engineering, Shiraz University, Shiraz, Iran
[b] Universidad de Málaga, Andalucia Tech., Departamento de Ingeniería química, Campus de Teatinos s/n, 29010 Málaga, Spain

ARTICLE INFO

Keywords:
Agricultural residue
Acid treated biomass
Fast pyrolysis
Porosity
Bio-oil
Syngas

ABSTRACT

This study reports the effect of heating rate and the addition of H_3PO_4 on the pyrolysis of three representative agricultural wastes of different lignocellulosic composition, namely pistachio shell, bitter orange peel, and saffron petal. Pyrolysis was carried out at 500 °C in a fixed-bed, lab scale reactor. Slow pyrolysis provided lower water contents in the liquid fraction. Fast pyrolysis increased the liquid yield for all the feedstocks, promoting the formation of phenolic, ketone/aldehyde compounds. It also enhanced the formation of water for all the agricultural residues. In addition, the energy content in the gas fraction is promoted due to a higher concentration of light hydrocarbons, methane, and hydrogen. However, when high inorganic matter is found in the feedstocks, the formation of CO_2 is favored, hindering the energy improvement. The treatment of the biomass with H_3PO_4 significantly increased the solid fraction, producing a huge porosity development in the char (surface area over 1600 m^2/g in pistachio shell product), at the cost of liquid fraction, which is mostly composed of water, with small amounts of acetic acid, phenol and toluene. The results pointed out that pyrolysis of agricultural waste can be targeted to achieve different products by switching pyrolysis conditions such as the heating rate and the treatment of the biomass with H_3PO_4.

1. Introduction

The increasing world population and development brings higher energy demand, which leads to overconsumption of nonrenewable fossil sources. Exploiting these fossil fuels at high pace depletes their reserves and emits toxic gases (CO_x, NO_x, SO_x), which are harmful to humans and their environment [1,2]. Biomass is an abundant and cost-effective renewable energy, which is mostly found in every world region and can help in replacing the use of fossil fuels [3].

Agricultural residues, as lignocellulosic biomass, can be considered as an emerging source of energy and chemicals. In this study, three agricultural residues with different origin and composition, such as pistachios shell, bitter orange peel, and saffron petals are chosen to be used as feedstocks for their valorization into high value-added products. In the case of pistachio shell, the countries with the highest production of pistachios in 2019 were Iran (571,000 tons), the United States (484,000 tons), and Turkey (267,000 tons); their combined share was 88% of the total production of the world [4]. On average, the empty shell wastes, including the hard shell, form around 15% of the total product. As an example, an amount of 77,550 tons of waste including hard shells is formed only in Iran per year [5].

Citrus fruits are one of the most important agricultural products in the world. In Spain, nearly 6.5 million tons of citrus are produced per year, of which over 1 million tons waste are left annually [6]. Orange industry generates different residues in the form of seeds, pulp, and peel. Specifically, 20% of the orange is orange peel, so only in 2018 were more than 15 Mt of orange peel generated in the world [7]. Saffron is another agricultural product, whose industry produces high amounts of residues. Saffron production reached more than 350 tons in 2019 [8] and annually 194,445 tons of petals are wasted as part of the production process in Iran, which accounts for 90% of the world's cultivation area.

The most common biomass thermochemical conversion processes are gasification, combustion, and pyrolysis. During the latter process, biomass is thermally decomposed in an oxygen free environment to gas, liquid, and solid fractions [9–11].

Depending on temperature, heating rate, and residence time, the

* Corresponding authors.
E-mail addresses: hadianfa@shirazu.ac.ir (M.J. Hadianfard), mirasol@uma.es (J. Rodríguez-Mirasol).

https://doi.org/10.1016/j.jaap.2022.105724
Received 25 July 2022; Received in revised form 19 September 2022; Accepted 21 September 2022
Available online 23 September 2022

pyrolysis process can be grouped into three types: slow, fast, and flash pyrolysis. Slow pyrolysis is implemented at low heating rates and high residence times, within a temperature range of 400–700 °C, meanwhile fast pyrolysis occurs under higher heating rates, at temperatures around 500 °C, and low residence time of evolved gases. Flash pyrolysis is aimed to heat the biomass with a very high heating rate at a temperature range of 450–900 °C [12–14].

Fast pyrolysis is considered as one of the promising thermochemical technologies that provide sustainability in many aspects like energy, economy, environment, and well-being of society. This process has been performed on different biomass types such as wood, agricultural residues, and domestic industrial wastes [15]. During the fast pyrolysis process, biomass is decomposed to vapor/gas and solid residue. The vapor is quickly cooled to room temperature for avoiding secondary cracking reactions, and therefore leads to an increase of the liquid fraction, which contains different organic compounds with a wide range of molecular weights and its composition and quality are heavily dependent on the composition of biomass feedstock. Bio-oil is an intermediate product, which can be easily stored and transported to be processed for fuel and chemicals production [16].

Even though fast pyrolysis is thoroughly studied in the literature, the systematic comparison between slow and fast pyrolysis of varied agricultural residues is not deeply analyzed, with only a few examples being found in the literature. In this context, Taib et al. investigated the fast pyrolysis process to produce the bio-oil from of banana pseudo-stem, which at optimum conditions (T = 500 °C and residence time=1.02 s) total liquid yield of 39.4 wt% was obtained [17], however, the distribution of products of slow pyrolysis is not reported. In another study, in the slow and fast pyrolysis of Cherry seeds (CWS) and cherry seeds shells (CSS), maximum bio-oil yields were about 44 wt% at 500 °C for both biomasses, whereas the bio-oil yields obtained under slow pyrolysis for SWS and CSS were 21 and 15 wt%, respectively; a fluidized bed reactor was used for fast pyrolysis experiments, while slow pyrolysis was studied in a fixed bed reactor [18]. Yang et al. also investigated the fast and slow pyrolysis of different parts of eastern redcedar under fast and slow pyrolysis at 450 and 500 °C; a pyrolysis probe attached to GC-MS is used to simulate fast pyrolysis, while slow pyrolysis is performed in a high-pressure batch reactor [19].

On the other hand, pretreatment of biomass is sometimes performed before pyrolysis in order to extract value-added compounds, modify the density or adapt the composition for achieving optimal results. For instance, treatment of the raw materials with acidic and alkaline agents affects the structure of the biomass, which changes the product yields distribution and properties of each pyrolysis product [20–22]. Various chemical agents, such as H_2SO_4, NaOH, KOH, $ZnCl_2$, and H_3PO_4, have been used for this aim [23]. One of the most striking features of chemical treatment is producing solid, known as activated carbon, with high surface area and pore volume as well as the presence of surface functional groups. For example, activated carbon from different agricultural wastes such as pistachio shell [23], date pits [24], jackfruit peel [25], and orange skin [26] has been already produced by chemical activation of different agricultural wastes such as pistachio shell [23], date pits [24], jackfruit peel [25], and orange skin [26]. Since most efforts are devoted to study the properties of the pyrolysis solid product, little is known about the composition and yields of liquids and gas phases obtained as coproducts in these treatments [27,28].

The objective of this study was to determine the potential benefits of fast and H_3PO_4-treated pyrolysis to improve the production of bioenergy and products with higher added value in the valorization of residual biomasses. Bearing this aim in mind, the slow, fast, and catalyzed pyrolysis with H_3PO_4 are performed using a similar fixed-bed reactor configuration, so that meaningful comparison between processes can be drawn. Such a study could bring light into which lignocellulosic feedstocks are more adequate for the production of the different pyrolysis products, when moving from slow to fast pyrolysis, or even catalyzed slow pyrolysis. Considering the importance and great volume of residues produced from pistachio, bitter orange and saffron, representative raw material of three major families of agricultural residues: nutshells, fruit skin and petals, as well as their different lignocellulosic composition, these wastes were chosen as models of three different families of agricultural residues (shells, peels, and petals) for validating the conclusions for a wide range of raw materials. For obtaining a good picture of the effects of these variables on the pyrolysis process, attention to the full characterization of the whole products is needed. Furthermore, in order to evaluate their potential as energy products, the yields and heating values of the different fractions have been also determined. In addition, the composition and porosity of the solid fractions have been also characterized for assessing their potential use as adsorbents. Apart from these, the distribution of pyrolysis products of saffron petals under different conditions is reported for the first time.

2. Materials and methods

2.1. Material preparation

Raw materials were Pistachio shell (PS), bitter orange peel (OP), and saffron petal (SP). PS and SP were provided from Khorasan Razavi, northeast of Iran, and OP was gathered from Fars province, south of Iran. Prior to their use, the feedstocks were dried at 105 °C in an air-dry oven for 12 h to remove the moisture. The dried samples were then milled and sieved to a particle size between 300 and 500. The prepared samples were stored in plastic flasks for their future uses. The physicochemical of the biomasses are reported in Table 1. More information can be found in our previous work [29]. Regarding SP biomass, to our knowledge, there is no published work on the content of the biopolymer components in the literature, except a study conducted by Fahim et al., who reported the results based on the dry weight (% w/w) as 10.2 protein, 8.8 fiber, 7.0 ash, 5.3 fat [30].

The acid-treated process was as follows: The prepared samples from the previous step were impregnated by incipient wetness with 85% (w/w) H_3PO_4 aqueous solution at room temperature and dried overnight at 60 °C in an oven. The impregnation ratio, R, (H_3PO_4/ precursor mass ratio) was set to 3 in accordance with a previous study regarding the preparation of H_3PO_4-activated carbons from orange peel [33].

2.2. Ultimate and proximate analysis of the raw materials

The elemental analysis was verified by a TruSpec micro CHNSO (Leco) analyzer to determine the mass fractions of carbon, hydrogen, nitrogen, and sulfur. The proximate analysis of biomasses was performed by a thermogravimetric analyzer (Q500, TA Instruments, USA) [34]. In the thermogravimetric analysis (TGA) experiment, 10 mg from each sample was loaded into the platinum container, and then heated from ambient temperature to 900 °C at a heating rate of 10 °C/min under a flow rate of 60 mL/min of nitrogen as carrier gas. At that point, carrier gas is switched to air and the temperature is held until constant weight is obtained.

2.3. Experimental setup

2.3.1. Slow and H_3PO_4-treated biomass pyrolysis experiments

The experiments for slow and H_3PO_4- treated biomass pyrolysis were performed under nitrogen atmosphere (flow rate: 150 mL/min STP) using a vertical tubular reactor (diameter: 2 cm). The reactor was loaded with a bed of 2–3 g of the selected feedstock, which was hold in the isothermal zone of the reactor using a compacted quartz wool layer. The experiments were carried out under atmospheric pressure, at 500 °C and at a heating rate of 10 °C/min. The bed temperature was tracked using an internal thermocouple. After pyrolysis, the furnace was cooled down to room temperature. The solid residue was recovered from the reactor at the end of the experiment, whereas the bio-oil was obtained at the reactor outlet from a condenser at ca. 0 ºC (mixture of acetone and ice is

Table 1
Physicochemical composition of different lignocellulosic biomasses.

	Proximate analysis (wt%)				Ultimate analysis[a] (wt%)					biochemical composition [31,32]				
	M	VM	Ash	FC	C	H	N	S	O[b]	Ce	HC	L	P	EX
PS	2.3	78.1	0.4	19.2	48.1	6.4	0.1	< 0.1	45.4	51.2	21.5	21.5	–	5.8
OP	1.0	67.5	4.9	26.6	44.4	6.2	1.0	0.1	48.3	25.1	10.2	4.3	34.0	26.4
SP	2.5	65.8	6.4	25.3	49.1	6.5	2.0	2.0	40.4	–	–	–	–	–
	Composition of ash (wt%)													
	K		Ca			Mg			P			Si		other
PS	0.1		–			–			–			–		0.2
OP	1.9		2.1			0.4			0.1			–		0.3
SP	3.0		0.6			0.5			0.7			0.5		0.9

M= moisture, VM= volatile material, A=ash, FC=fixed carbon.
Ce=cellulose, HC=hemicellulose, L=lignin, P = pectin, EX=extractive.
[a] dry-ash free (daf) basis.
[b] was calculated by difference. O = 100 – C – H – N – S.

used as coolant). The experiments were repeated at least three times for each biomass in each process. The mass of liquid product and solid residue (char) were weighted, and the gas yield was confirmed by difference.

2.3.2. Fast pyrolysis experiment

Fig. 1 shows the schematic diagram of the system used in the fast pyrolysis process. The same reactor described in the previous section is used in this system. On the top of the reactor, biomass was loaded inside a dropper consisting of a 4 cm height chamber with 25 mm of internal diameter, gas inlet and outlet for purging of the chamber, and two ball valves for dropping biomass inside the heated reactor and loading new biomass into the dropper. Inside the reactor, a biomass holder zone consisting of a quartz wool layer was placed in the isothermal region so that biomass can be dropped into the previously heated reactor. An additional layer of 5 g of silicon carbide was used as an inert heat carrier. The reactor was mounted inside an electrical vertical furnace and was insulated to minimize heat loss. The experiment was performed under nitrogen atmosphere (flow rate: 150 mL/min STP) and the bed temperature was tracked using an internal thermocouple. The effect of using different biomass loadings on the reactor temperature was also studied. A thermocouple attached to a data logger was placed on top of the SiC layer for this purpose. The temperature of the bed was 495 °C after one second when 100 mg of biomass were dropped into the reactor. Under these conditions, the heating rate was estimated to be higher than 100 °C/s. In accordance with this finding, the fast pyrolysis experiments consisted of 8–10 sequential drops of 100 mg of the chosen biomass. The interval between the different loadings was 2–3 min, time necessary to obtain a negligible CO and CO_2 evolution. While the biomass of the previous loading was being pyrolyzed, a new biomass sample was loaded in the dropper through the top valve and purged with nitrogen before being introduced into the reactor. Regarding the recovery of the products, the reactor was connected to two cooled condensers to gather the bio-oil. The biochar was collected from the reactor after the experiment was finished.

2.4. Analysis of products

2.4.1. Analysis of bio-oil composition by GC/MS

Bio-oil was recovered from the condenser at the outlet of the pyrolysis reactors. The bio-oil was dissolved in acetone (analytical grade, Sigma-Aldrich) in 1:100 vol ratio. All the resulting mixtures were analyzed by Gas Chromatography–Mass Spectrometry (GC/MS), using an 7000D GC/MS Triple Quad (Agilent Technologies, USA), equipped with an Agilent DB-624 column (60 m × 0.250 mm×1.4 μm) and HP-5 ms column (30 m × 0.250 mm×0.25 μm), FID and mass spectrometer detector (MS). Ions were detected in full scan mode (mass range from 15 to 400 *m/z*), with an electronic impact of 70 eV. Identification of compounds was achieved by comparing the mass spectra with the NIST MS Search 2.0 mass spectral library. The water content in the bio-oil was

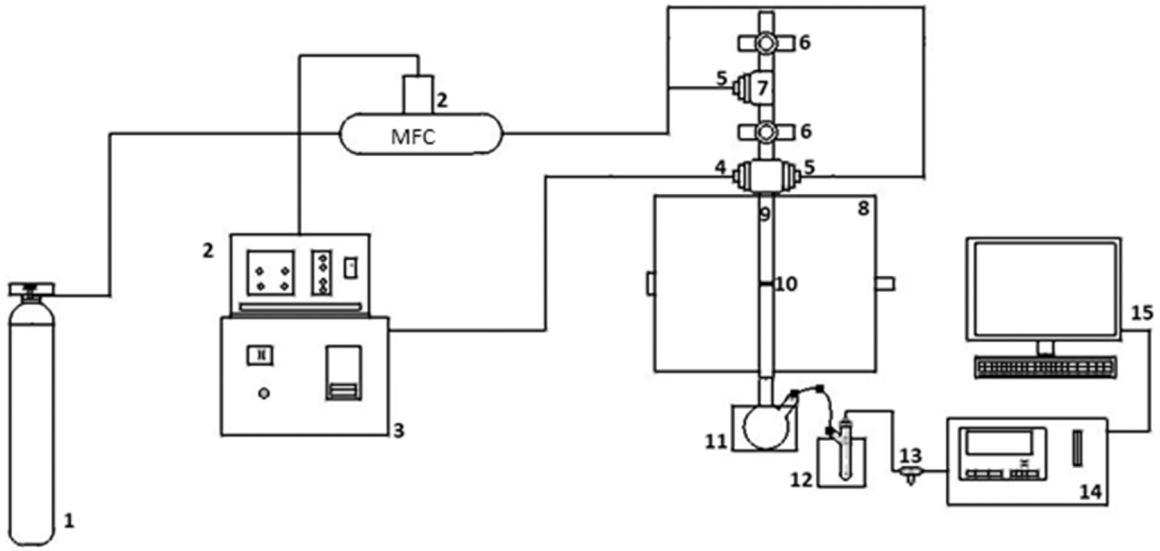

Fig. 1. Schematic of the fast pyrolysis set up (1) nitrogen cylinder (2) mass flow controller (3) temperature controller (4) thermocouple (5) N_2 inlet (6) ball valve (7) biomass dropper (8) reactor (9) pyrolysis furnace (10) quartz wool (11) first condenser (12) second condenser (13) three-way gas collecting (14) NDIR sensor (15) computer.

measured by Karl-Fisher titration (KF V20, Mettler Toledo). Bio-oil acidity was determined using a pHmeter (HI8424, Hannah).

2.4.2. Analysis of the non-condensable gases

Analysis of the gas fraction from slow and H_3PO_4-treated biomass pyrolysis experiments was performed at the condenser outlet. The gas composition was determined with a Perkin Elmer Auto system GC equipped with a packed column (Hayasep-D 100–120 mesh, PE) with FID and TCD detectors. Identification and absolute quantification were carried out by external calibration with a standard commercial mixture of gases obtained from Linde.

The gases evolution from the fast pyrolysis was analyzed with two analyzers. CO and CO_2 concentrations were determined online by a non-dispersive infrared (NDIR) gas analyzer (Siemens Ultramat 23). Hydrogen, methane, and light hydrocarbons (C_2-C_3) were determined offline by injecting the gas stored in the gasbag into a Perkin Elmer Auto system GC equipped with a packed column (Hayasep-D 100–120 mesh, PE) with TCD and FID detectors.

The LHV values have been determined following the equation deduced by Lv et al. [35].

2.4.3. Analysis of the solid fraction

In order to analyze the solid fraction obtained from the acid treated samples, the excess of phosphoric acid was removed by washing with distilled water at 60 °C until neutral pH and negative phosphate analysis in the eluate. The respective solids obtained are denoted as PSC, OPC and SPC.

A truspec micro CHNSO analyzer, from Leco was used to determine the mass fractions of carbon, hydrogen, nitrogen, and sulfur for the elemental analysis. Proximate analysis was carried out to calculate the moisture contents, fixed carbon, volatile matter, and ash contents. This analysis was conducted by using a thermogravimetric analyzer (TGA/DSC1, from Mettler Toledo). The higher heating value (HHV) of the solids was calculated based on the following equation derived from Cordero et al. [36].

$$HHV = 0.3543 \times FC + 0.1708 \times VM \quad (\frac{MJ}{kg}, dry \quad basis) \tag{2}$$

where VM stands for volatile matter (%) and FC is fixed carbon (%) in the solid.

The porous structure of the solid fractions was characterized by N_2 adsorption–desorption at − 196 °C and by CO_2 adsorption at °C. The measurements were performed in an ASAP 2020 model equipment of Micromeritics. Prior to the experiments, the samples were degassed overnight at 150 °C. From the N_2 adsorption isotherm, the apparent surface area (S_{BET}) was calculated by applying the BET equation. Consistency criteria as suggested by Rouquerol was applied to ensure that BET values are properly reported [37]. Application of the Dubinin-Radushkevich method to the N_2 and CO_2 adsorption isotherm provided the micropore volume (V_{DR}^{N2} and V_{DR}^{CO2}). Finally, the mesopore volume (V_{mes}) was calculated as the difference between the adsorbed volume at a relative pressure of 0.96 and the micropore volume (V_{DR}^{N2}).

3. Results and discussion

3.1. Yield of products

Fig. 2 shows the yield of the corresponding products for the different type of pyrolysis for PS, OP, and SP. Fast pyrolysis shows higher liquid yields compared to those obtained by slow pyrolysis. The high bio-oil yields derived from fast pyrolysis are due to its high heating rate and short gas residence time, which enhance the rapid fragmentation of biomass and mitigate the secondary cracking of tar [18,38]. Higher bio-oil fractions under fast pyrolysis were also reported by Pütün et al., which studied the slow and rapid pyrolysis of pistachio shell in a tubular reactor. Temperature, heating rate and nitrogen flow were variable parameters in their work. The highest bio-oil yield was 27.7% when temperature, heating rate and nitrogen flow were 500 °C, 300 °C/min, and 100 cm^3/min, respectively [38]. The superior yield obtained at the same temperature (almost double, 53 wt%) is probably related to the shorter residence time of gas in this system (aprox. 2 s for the isothermal region in the system herein used), which avoids secondary cracking reactions. In the case of bitter orange peel, no direct comparison using a similar system can be found in the literature. Alvarez et al. reported bio-oil yields of ca. 55% wt and char yields of 27–33% for fast pyrolysis of citrus waste using a conical spouted bed reactor [39], whereas Aguiar et al. studied slow pyrolysis of orange peel in fixed bed pyrolysis at different temperatures, obtaining char yield of 28–29% and liquid yields of ca. 40%, with a large content of water, at 450 ºC [40]. The larger liquid yield obtained in the latter work was probably related to a much higher moisture content of 7% wt. in the raw material, which could also explain the large water content on the obtained bio-oil. After subtracting the content in moisture, an estimated liquid yield of around 34% is obtained from the data reported by Aguiar et al. [40], being in line with the ones reported in this work. On the other hand, the superior spouted

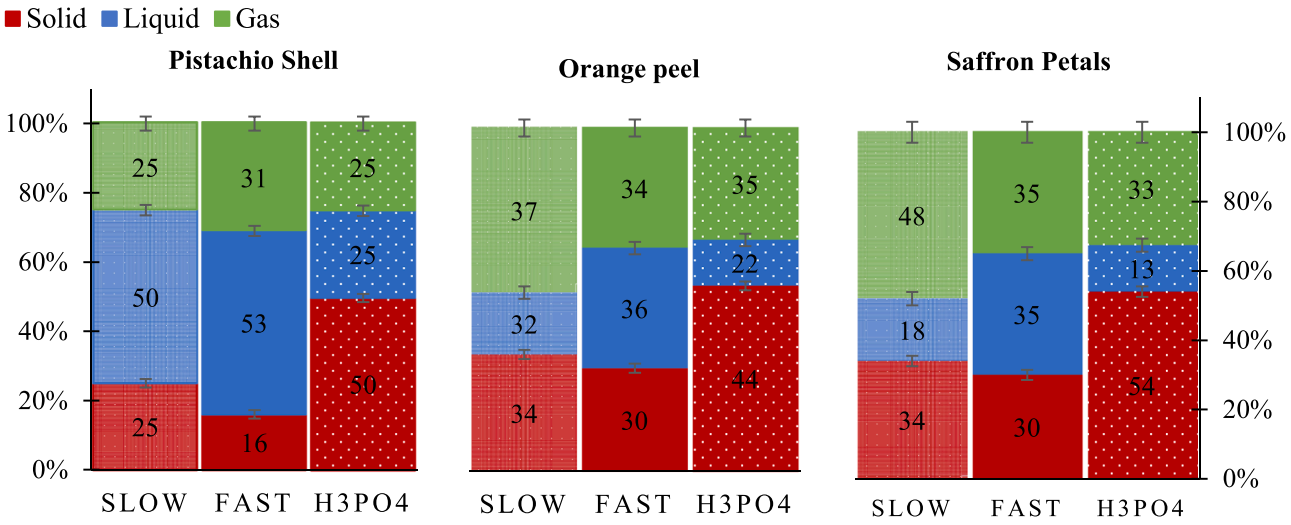

Fig. 2. Compared product distribution yields for PS, OP and SP pyrolyzed at 500 ºC under slow conditions (10ºC/min), fast conditions (>100 ºC/s) & H3PO4-treated conditions.

bed reactor technology, with lower residence times for the gases and improved mass and heat transfer make possible to achieve much larger bio-oil yields [39] than the fixed bed reactor technology used in this work. To our knowledge, no pyrolysis data of saffron petals is currently available for comparison purposes. Only a few comparable works can be found, such as that of Sriram and Swaminathan about pyrolysis of Musa balbisiana flower petals. However, they only used thermogravimetric analyses and did not provide any information about the distribution of the products [41].

Regarding the results for different biomass, SP biomass gives maximum solid yield, while PS produces higher amounts of liquid and OP a higher yield of gas. This different behavior among the biomasses can be associated with their chemical structures and ash content. The aromatic and carbon-rich structure of lignin is the main contributor to the solid fraction (i.e., char) of pyrolysis processes, followed by pectin [42] and hemicellulose [43]. The results of XRF analysis of OP and SP (Table 1) show high amounts of Ca and K, which facilitate secondary reactions in favor of higher gas formation. These elements catalyze pyrolysis reactions, and they fasten the interaction between different products causing higher gas evolution [44,45]. According to previous research, potassium (K) improves the cracking of the glucosidic unit of cellulose to lower molecular weight compounds through depolymerization and fragmentation, which results in more water formation, CO_2, methane, acetone and acetic acid, among others [46].

It is also interesting to note that the composition of the raw material has a critical impact on the product distribution, independently of the kind of pyrolysis carried out. The solid yield of cellulose-rich pistachio shells is severely decreased in fast pyrolysis, probably as the outcome of associated cellulose depolymerization reactions proceeding at faster rate than charring and repolymerization ones. As cellulose content is lower in OP and SP, the impact on the solid yield of fast pyrolysis is less important. It is also worth noting that the secondary cracking reactions from vapors of orange peel and especially of saffron petals, which are probably behind the higher gas evolution on this feedstock, are noticeably suppressed in fast pyrolysis, increasing the corresponding liquid yield.

The impregnation of biomasses with phosphoric acid has a considerable effect on the thermal decomposition of the biomasses, which alters the yields to the different pyrolysis products. Compared to slow and fast biomass pyrolysis, bio-oil formation is strongly restricted, while the formation of solid is considerably increased. Phosphoric acid catalyzes the hydrolysis of the glycosidic linkages in hemicellulose and cellulose, and it also cleaves aryl ether bonds in lignin [47] at low temperatures. As temperature increases, the organic species formed after the hydrolysis of the biopolymers can be combined with phosphorus species to form phosphate linkages. Such bonds serve to crosslink and connect the fragments of biopolymers, effectively binding volatile matter into the carbon product and, hence, delivering a net increase in carbon yield during pyrolysis, at the cost of the liquid fraction [44,47–50]. Since the main phosphoric acid interaction with lignocellulosic biomass proceeds through cellulose, the highest increase in solid yield is achieved in cellulose-rich PS. On the other hand, the main building blocks of pectins on OP are either native or methylated α-D-galactopyranosyl acid units [51], which have low reactivity with phosphoric acid, and therefore, deliver a lower increase in solid yield.

3.2. Analysis of gas fraction

Fig. 3 shows the yield fraction of gas compounds in the different types of pyrolysis for PS, OP and SP. The gases consisted mainly of carbon monoxide (CO), carbon dioxide (CO_2), methane (CH_4), hydrogen (H_2), and small amounts of light hydrocarbons (C_2-C_3). Occurrence of several reactions such as decarboxylation, dehydrogenation, decarbonylation, and hydrocarbon cracking during the pyrolysis process give rise to evolution of these gases. CO and CO_2 are related to the presence of oxygen in the biomass and are generally produced because of

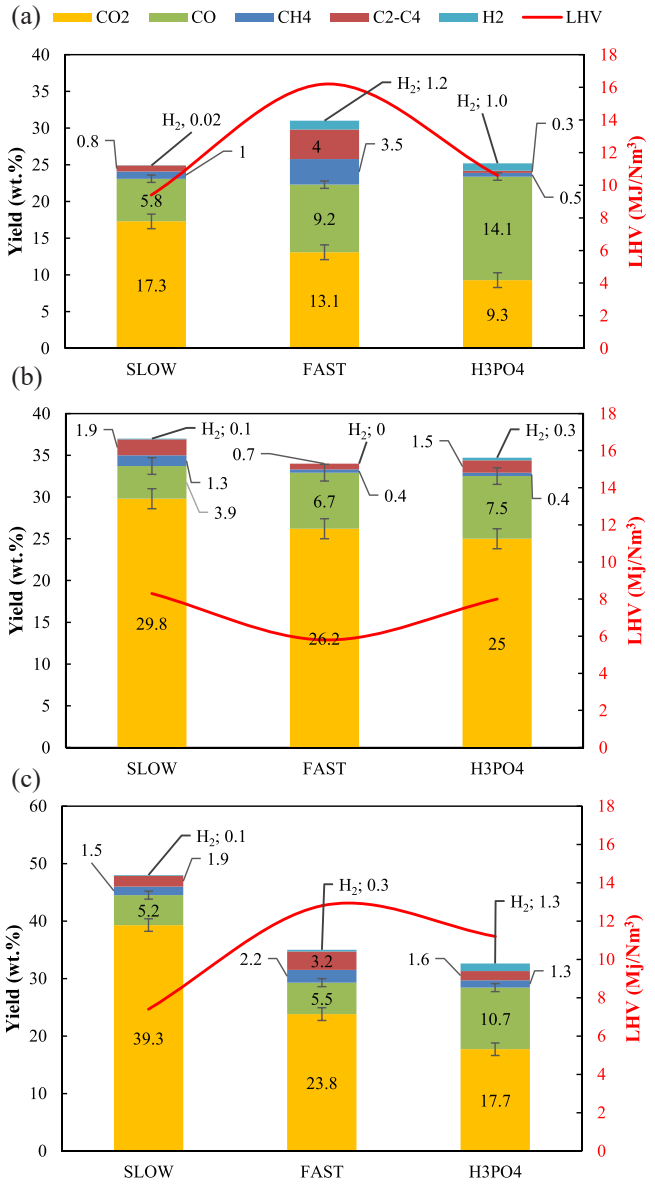

Fig. 3. Influence of the pyrolysis process at 500 °C in gas composition in (a) PS, (b) OP, and (c) SP under slow (10°C/min), fast (>100 °C/s) & H_3PO_4-treated conditions.

decomposing and rearranging of carbonyl (C═O), hydroxyl (C-OH), ether (C-O-C) and carboxylic group (COO) from holocellulose and pectins. These are the main components of gas fraction in all these cases. CH_4 is generated due to the decomposition of methoxy (-O-CH_3) and methylene (-CH_2-) groups, which are found on lignin and methylated pectins, while cracking and dehydrogenation of heavier hydrocarbons, which mainly occur at higher temperatures, leads to H_2 production [52, 53].

When comparing the gas amounts between the biomasses, it is seen that PS produces more CO. On the other hand, CH_4, C_2-C_3, and H_2 are obtained in higher amounts in SP, with OP pyrolysis gases showing a similar composition to SP. CO evolution is mostly connected to the presence of hemicellulose and cellulose, which is larger in PS. Conversely, CO_2 evolution is related to the presence of hemicellulose and pectins, explaining the higher occurrence of this gas in the pyrolysis of OP and SP. Contrarily, the formation of C_2-C_3 and H_2 is associated with lignin decomposition and charring reactions, with lignin being found in larger quantities in PS.

These trends are strongly affected by the kind of pyrolysis performed

(fast or acid-treated). It has been found that fast pyrolysis leads to increasing light hydrocarbons, hydrogen, and methane when compared to slow pyrolysis. The higher contribution of CH_4 and H_2 in fast pyrolysis has been also observed for sugarcane bagasse at 500 °C [54], although scarce information regarding the effect of fast pyrolysis on C_2-C_3 gases can be found. The results herein reported seem to point out that the increasing trend is validated no matter the composition of the feedstock, with PS reaching the highest values of hydrogen and C_2-C_3 light hydrocarbons, which are probably obtained as the outcome of ring-opening reactions from the anhydrosugars monomers formed by cellulose depolymerization. Given that fast pyrolysis leads to a larger yield of the gas fraction, it is reasonable to think that highly reactive cellulose monomers, which could have faced charring and repolymerization reactions during slow pyrolysis, are actually cracked at fast pyrolysis, shifting the yield from solids to gas.

Differently, gas evolution from pyrolysis of H_3PO_4-treated biomasses shows higher contents of hydrogen and CO (syngas) compounds. In the presence of phosphoric acid, oxygen is not only removed from biomass as carbon oxides; hydrogen is also liberated as hydrogen molecule by secondary methane formation [47]. Furthermore, the decrease of CO_2 also indicates that hemicellulose, as the main contributor of CO_2, is cracked to a lesser extent than cellulose, probably due to the occurrence of crosslinking reactions that are promoted by phosphoric acid [48].

Interestingly, the H_2/CO molar ratio of the pyrolysis gas obtained by fast pyrolysis is as high as 3.7 for pistachio shell, while in the case of H_3PO_4-treated biomass pyrolysis, H_2/CO ratio is 3.3 for saffron petals, turning these streams as promising candidates for syngas upgrading, enabling their use as feedstock for the direct methanol synthesis or Fischer-Tröpsch process.

As observed in Fig. 3, the highest LHV values obtained from the fast pyrolysis of PS and SP are due to the formation of high amounts of light hydrocarbons, like methane. However, the evolution of these gases slightly decreased in the fast pyrolysis of OP, decreasing the LHV. Finally, the improvement in LHV observed in acid-catalyzed pyrolysis mainly come from a higher syngas (CO and H_2) generation. In addition, a higher LHV value is obtained for PS in this process.

3.3. Bio oil analysis

The composition of the liquid fraction recovered from the condensers related to the slow and fast pyrolysis is summarized in Fig. 4. The amount of water found in the bio-oil is between 44% and 78%, with the lowest water percentage obtained in slow pyrolysis for PS. Water content is higher for OP and SP independently of the heating rate used in the pyrolysis. Fast pyrolysis enhances the formation of water for all the agricultural residues, with relative increases between 9% (PS) to 28% (SP). Contrarily, the bio-oil pH value follows the order SP>OP>PS. SP bio-oil shows the lowest acidity value, 3.8, in agreement with the lower content of organic acids in the bio-oil, (see Acids family group composition in Fig. 4). The acidity of the bio-oil is mostly unaffected by the heating rate for PS and SP; however, fast pyrolysis of orange peel does decrease acidity of bio-oil (pH of 3.4 in fast pyrolysis vs 2.5 in slow pyrolysis). This finding is supported by a notable decrease in acid content in the composition of the organic phase of the bio-oil.

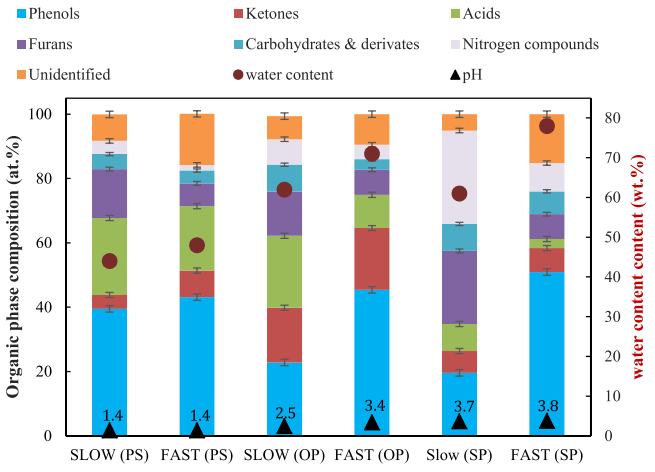

Fig. 4. Analysis of the pyrolysis liquid phase for three biomasses under slow and fast pyrolysis.

The compounds found in the organic phase of the bio-oils have been scrutinized using GC-MS, and the identified compounds have been grouped based on their functional groups, in a similar way to those reported in other works about pyrolysis of other lignocellulosic residues [55,56]. The detailed results are summarized in Tables S1–3.

Fast pyrolysis induces some differences in the composition among the families of the compounds. In general, phenol, and ketone compounds increase under the fast pyrolysis process for all feedstocks, while carbohydrates & derivatives, acid and furan compounds decrease. These trends fall in line with previous research for other lignocellulosic biomasses [19,57]. For instance, higher heating rates promote the formation of levoglucosan and hydroxyacetaldehyde along with a decrease in the yields of carboxylic acids [55].

Phenol and its derivatives are the principal compounds present in the bio-oil for all biomasses, Fig. 4. These compounds are mainly derived from the thermal degradation of lignin, which contains different aromatic units within its structure [58]. It is also important to note the large increase in phenols content obtained in SP under fast pyrolysis conditions. Phytochemical analysis has shown that saffron flowers are rich in antioxidant compounds like flavonols (kaempferol), flavanones, anthocyanins, crocins and crocetin [59]. Upon slow pyrolysis, flavanoids and anthocyanins, which are phenolic compounds, are probably facing charring reactions similar to those of lignin, contributing to the solid fraction. However, fast pyrolysis enhances the decomposition of the flavonoid dimers, thus increasing the phenol pool of the liquid fraction. Orange peel, which also has a high flavonoid content [60], shows a similar, but less intense, trend.

The main organic components of the bio-oil obtained under both processes for PS, are phenol derivatives, Fig. 4 & Table S1. Syringol has been found as the most abundant compound for both processes, with methoxyeugenol, 5-tert-butylpyrogallol, desaspidinol, acetophenone and acetosyringone, also found in large quantities.

In the case of OP and SP, fast pyrolysis delivers a huge increase in phenol derivatives, being this increase led by the rise of the syringaldehyde family of compounds (reaching values of 14% and 12.1%, respectively). Apart from that, OP bio-oil is also rich in resorcinol, phenol and m-, o- cresols, (taking up more than 4% of peak area). As for SP, syringaldehyde compounds are followed by phenols and catechol-type compounds, like p-, o-cresol, hydroquinone, or 2,4-xylenol.

These obvious changes in the aromatic product distribution must be related to the different nature of lignin between samples. Lignin in PS probably has a similar composition to those observed in hardwoods, based on syringol and guaiacol units; lignin in OP is probably mainly constituted by guaiacol and p-hydroxyphenyl units, meanwhile SP lignin should be composed mostly by the latter ones. The use of high heating rates seems to promote lignin depolymerization over cracking and charring reactions in all biomasses, explaining the huge increase in phenols derived from the monolignols. The presence of inorganic matter can also promote the charring reactions of lignin in SP and OP. When the heating rate increases, the slow crosslinking and condensation reactions that are catalyzed by the inorganic elements cannot take place, and monolignols and their derived phenols are released into the gas phase, explaining the large increase of these compounds in the fast pyrolysis bio-oils of SP and OP. The phenol and its derivatives are valuable and useful as a resin, to produce antioxidants, dye, and pharmaceuticals [61].

Acid compounds constitute a family unavoidably present in bio-oil.

Acids in the bio-oil fraction are attributed mainly to the decomposition of the acetyl groups present in hemicellulose [62] and pectin [63]. Acetic acid is the main compound in this group, whose concentration decreases significantly under the fast pyrolysis of all the biomasses. The amount of acids present in bio-oil of each biomass is consistent with the pH results, Fig. 4. Unfortunately, acidity is one of the main problems of bio-oil and its recovery by separation from bio-oil would allow their valorization as a by-product and would ease the use and upgrading of the acid-free bio-oil.

Another important family found in bio-oil is furan. Furanic compounds, especially furfural and 5-hydroxymethylfurfural are recognized as dehydration products of sugars [53]. The relative amounts found in this study are quite dependent on the feedstock and pyrolysis process. In this sense, SP pyrolysis produces the highest furan concentrations, whereas fast pyrolysis decreases their concentration for all residues. SP bio-oils are rich in 2(5 H)-furanone, 2,3-dihydrobenzofuran, furfuryl alcohol, 5-hydroxymethylfurfural, and dihydro-4-hydroxy-2 (3 H)-furanone. Differently, PS bio-oil is rich in furfural, while furfuryl alcohol, furfural, 5-hydroxymethylfurfural and 5-methyl-2-furaldehyde are detected in the liquid phase obtained from OP. Tables S1–3 show a decline in branched furans in bio-oils derived from fast pyrolysis, probably as a consequence of the promotion of secondary cracking reactions. In slow pyrolysis, hemicellulose decomposition and furan evolution take place at mild temperatures (250–350 ºC), avoiding the occurrence of secondary cracking reactions that probably take place under fast pyrolysis conditions at 500 ºC.

It has been found that fast pyrolysis promotes the formation of ketone compounds, with OP being the most suitable agricultural residue for the obtention of ketones, Fig. 4. The increase observed in fast pyrolysis seems to be connected to a larger formation of cyclopentanone compounds, a tendency that is confirmed for all the feedstocks no matter their biopolymeric composition, Tables S1–3. The ketone compounds are usually derived from hemicellulose and cellulose degradation, and it has been reported that they are formed during pyrolysis through the condensation of carbohydrates and decomposition of oxygenate compounds and furans due to secondary ring scission and deacetylation reactions of sugars and furans [64]. Compounds of this family can be also grouped according to their linear or cyclic structure. The formation of cyclopentanone, the most representative compound in the second group, has been attributed to hemicellulose decomposition [65], with the cyclic ketones being likely derived from the xylan present in stem by cleavage of the o-glucosidic bonds and subsequent removal of the hydroxyl groups of the xylose rings [66]. Another feature observed in the obtained bio-oil from fast pyrolysis is the conversion of aldehyde compounds into cyclic ketones, as can be seen in Tables S1–3.

Some saccharides are detected in PS and SP bio-oils. The maximum amount of this family is related to D-Allose, 4%, which appeared in PS bio-oil obtained under fast pyrolysis, Table S1. Beyond D-Allose, maltols are the next main component of bio-oils from OP and SP. These compounds are suggested to be obtained via dehydration and rearrangement of levoglucosan and 1,4:3, 6-dianhydro-α-D-glucopyranose, which is known to happen at low temperatures (200 ºC) during the pyrolysis of sucrose or starch [67]. Their low contribution to the bio-oil fraction can be related to their low thermal stability, which favors their decomposition into different oxygenate compounds, such as furans, ketones and aldehydes. Accordingly, these compounds are likely degraded under fast pyrolysis conditions, explaining the decline observed in Fig. 4.

The amounts of N-containing compounds are in the order SP>OP>PS, consistent with the nitrogen content reported in the elemental analyses of the feedstocks, Table 1. According to previous research, the formation of these compounds is related to the interaction between proteins and carbohydrates. Amino acids are usually more reactive than other compounds, being prone to react with active cellulose and derived compounds such as hydroxypropanone. For instance, pyrolysis of glutamic acid in lignocellulosic biomass leads to pyrrolidinone compounds [68], which are found in orange peel. Pyrolysis of proteoglycans at temperatures over 500 ºC can also generate pyridines, pyrroles, and similar N-aromatic compounds [65]. The generation of compounds such as methyl L-pyroglutamate, i.e., the main nitrogen-containing specie found in SP, Table S3, has been reported for direct pyrolysis of amino acids, meaning that protein concentration should be rather high in saffron petals for enabling their formation, as reported elsewhere [69]. Finally, the production of N-compounds has been also reported as feasible in raw materials with low N-content, such as cellulose and cellobiose [70], obtaining oxazolidine and other compounds resembling those observed in PS bio-oil, Table S1, but in very low amounts. Therefore, the formation of N-derived compounds is largely dependent on the presence of proteins, proteoglycans, amino acids and other N-containing species in the feedstock [39,71]. It should be pointed out that the bio-oil obtained under fast pyrolysis has much lower concentration of nitrogen compounds. It seems like amino acids decomposed during fast pyrolysis could be incorporated into the char forming pyrroles, pyridines, and quaternary nitrogen [72]. In fact, elemental analysis of SP char obtained by fast pyrolysis confirms the presence of nitrogen, reaching 2.8% wt. The presence of such high nitrogen concentration can be of interest for certain electrochemical applications [73]. Generally, after upgrading the bio-oil can be used in different application such as biofuel or feedstock for oxygenates, hydrocarbons (olefins/aromatics) or hydrogen, or application in the production of carbon materials, asphalts, pesticides, fertilizers, perfumes, polyurethane foam or plastic [74].

Table 2 summarizes the detected compounds in the liquid phase obtained from H_3PO_4-treated biomass pyrolysis together with their water content and pH values. When the biomasses are treated with H_3PO_4, the obtained liquid phase is completely different from those of slow and fast pyrolysis, starting by the clearer, aqueous-like appearance. As previously discussed, condensation reactions catalyzed by H_3PO_4 proceed particularly through dehydration reactions. It is also important to remark that phosphoric acid contains 15% wt. of water. Thus, a huge increase in water content is found in these bio-oils, Table 2. Moreover, the pH value is slightly increased (see the differences in pH in Fig. 4), since, probably, part of phosphorus leaves the reactor as phosphoric acid ester compounds (as pointed out by the presence of phosphoric acid, diethyl pentyl ester, Table 2), which are hydrolyzed in the bio-oil, increasing acidity. In addition, this process seems to demote the release of organic volatiles, with the liquids consisting of only a few

Table 2
Composition analysis of liquid-phase obtained from H_3PO_4 acid treatment.

Compounds	Biomass		
	PS	OP	SP
	Amount (area %)		
Acetic acid, butyl ester	85.9	48.6	35.6
Acetic acid	4.6	10.5	17.8
Toluene	4.1	20.1	16.4
Phenol	4.3	10.2	14.4
Phenol, 4-methyl-	0.0	4.9	6.8
Phenol, 3-methyl-	0.0	2.1	2.8
3-(Methoxymethoxy)butanoic acid	0.0	0.0	2.7
Phosphoric acid, diethyl pentyl ester	1.1	3.6	2.0
Furan, 2-ethyl-5-methyl-	0.0	0.0	1.4
pH	1.3	2.4	2.6
Water (%wt.)	88	83	88

particular products. It is important to note that the concentration of these compounds is low, since the liquid fraction obtained in acid treated pyrolysis has less than 15% in organic compounds (see water composition in Table 2). As can be seen in Table 2, acetic acid and acetic acid derived esters are the main compounds found in the three biomasses. Next to them, the aromatic family of compounds, with toluene, phenol, and phenol derivatives as the major chemicals, are detected in large amounts in SP and OP bio-oils. Interestingly, ketone, furans, carbohydrates and N-containing compounds are not found in relevant amounts in the bio-oil, pointing out that phosphoric acid is promoting the incorporation of cellulose, hemicellulose and amino acids -derived compounds in the solid fraction of the pyrolysis products. Moreover, these results are also showing that the selectivity of the products in the bio-oils obtained from acid treated biomass is somehow improved. In this sense, Lobos et al. pyrolyzed a Kraft pulp waste with H_3PO_4. Their selectivity to bio-oils was particular and they claimed that only levoglucosenone (LGO) was achieved [75]. The higher amount of H_3PO_4 and higher pyrolysis temperature used in this work seem to shift the selectivity towards different products.

3.4. Analysis of solid fraction

The ultimate and proximate analyses and the higher heating values (HHVs) of the solid fraction for each biomass obtained from different types of pyrolysis are compiled in Table 3. Fixed carbon increases under fast pyrolysis, while moisture, volatile material, and ash contents decrease compared to slow pyrolysis. Acid treatment gives rise to solids with higher moisture and fixed carbon contents and lower volatile and ash amounts. As for proximate analysis, the solids show similar carbon, nitrogen, and sulfur composition independently of the heating rate used, but fast pyrolysis provides a slightly higher amount of oxygen [18]. It is also interesting to note that hydrogen content declines with phosphoric acid treatment in OPC and SPC solids, confirming the higher H_2 releases observed in Fig. 3. The presence of high amounts of nitrogen, oxygen and ash in the solid residues from OP and SP makes feasible their possible use as raw material for the preparation of catalysts and soil improvers [76–78]. For instance, Yao et al. studied the performance of a Ni/ char catalyst for biomass gasification, achieving a high H_2 yield of 64 vol%, 92.08 mg g^{-1} biomass at the optimum operation conditions [77].

HHV of the solids has been determined from their proximate analysis using Eq. (2). The obtained values are in the range of 21–33.5 MJ/kg. According to Table 3, the maximum HHVs are obtained under the pyrolysis with H_3PO_4-treated biomasses, which is due to the removal of large quantities of ashes during the washing step. Differently, fast pyrolysis has a low impact on HHV. Comparing the different feedstocks, the best results in terms of HHV are obtained for solids from PS, due to the higher amount of fixed carbon and lower amount of ashes compared to their counterparts. The energy content of OP solids shows medium values, like those reported for charred wood, while PS solids are in the upper range of HHVs, being close to those reported for biochar obtained from straw [79]. Finally, SP shows poorer HHV values owing to the high amount of inorganic matter (i.e., ash content) in their composition.

Fig. 5 shows the N_2 adsorption–desorption isotherms at − 196 °C for the three solid fractions obtained from acid treated biomass pyrolysis. The N_2 uptake of the solid residues (chars) from slow and fast pyrolysis are negligible due to the poor and narrow microporosity development, which is not accessible for N_2 adsorption at − 196 ºC, and therefore they are not included.

In general, all the N_2 adsorption isotherms reported in Fig. 5 shows notable N_2 uptake at very low relative pressures followed by monotonous increase in the quantity of N_2 adsorbed as relative pressure increases, which are regarded as type I + type IV isotherms according to IUPAC classification [37], corresponding to a well-developed microporous structure with a significant contribution of mesoporosity. The isotherm from the SPC sample presents the lowest N_2 uptake at low relative pressures and the lowest slope of the isotherm at medium and high pressures. The appearance of small H4 type hysteresis loop (no limited adsorption at relative pressures close to 1) indicates the presence of narrow slit-shaped pores. The OPC and, especially, PSC show a significantly higher contribution of mesoporosity, as revealed by the higher N_2 volume adsorbed at medium-high relative pressures and the larger hysteresis loops. In the case of PSC, H1 type hysteresis with certain contribution of H4 is observed, indicative of narrow mesopores, while the H2 type hysteresis loop of OPC (i.e. steeper slope of the desorption with respect to the adsorption isotherms) suggests the presence of a broad mesopore size distribution of varied shapes [37].

The textural parameters of the porous structure of the different

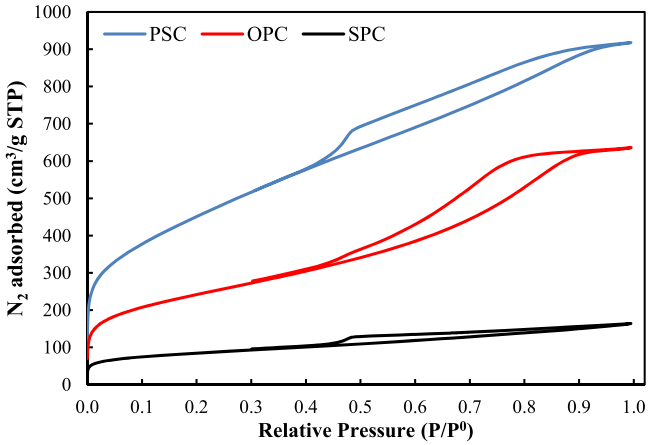

Fig. 5. N_2 adsorption–desorption isotherms at − 196∘C of solid residues obtained from the acid treated biomass pyrolysis.

Table 3
Ultimate and proximate analysis and HHV values of chars for all the pyrolysis processes.

Sample	Proximate analysis (wt%)				Ultimate analysis (daf[a], wt%)					HHV (MJ/Kg, dry basis)
	M	VM	FC	ash	C	H	N	S	O[b]	
PS (slow)	4.0	23.3	70.4	2.3	88.5	3.1	0.1	0.1	8.2	30.1
OP (slow)	8.5	28.0	50.7	12.8	78.2	3.5	2.2	0.0	16.1	24.9
SP (slow)	6.5	24.7	44.2	24.6	82.1	3.3	3.2	0.8	10.6	21.3
PS (fast)	2.8	15.9	79.5	1.8	87.3	3.4	0.1	0.0	9.2	31.8
OP (fast)	5.6	24.9	54.0	15.5	77.2	3.8	2.3	0.1	16.6	24.8
SP (fast)	4.4	23.1	52.0	20.5	79.9	3.2	2.8	0.1	14.0	23.4
PSC	12.2	5.9	80.1	1.8	94.8	2.5	0.2	0.0	2.5	33.5
OPC	10.8	8.1	70.5	10.6	84.1	1.9	0.4	0.0	13.6	30.5
SPC	6.5	5.2	77.7	10.6	86.2	1.7	2.8	0.2	9.1	30.4

M=moisture, VM= volatile material, FC= fixed carbon.
[a] dry ash free.
[b] calculated by difference.

solids, obtained from the N_2 and CO_2 isotherms, are summarized in Table 4.

In the case of slow and fast pyrolysis, all the solids have $V_{CO2}>V_{N2}$ (Table 4), with the largest CO_2 micropore volume being attained in PS char obtained at slow pyrolysis. This difference between isotherms can be explained by diffusional limitations of N_2 during adsorption at − 196 °C in narrow micropores (those with sizes under 0.5–0.7 nm). Even though the CO_2 molecule presents a similar kinetic diameter to N_2, the temperature for the determination of the CO_2 adsorption isotherm, 0 °C, boosts the diffusion rate in narrower micropores, enabling it to reach the adsorption equilibrium in shorter times. Thus, all the slow and fast pyrolysis solids have narrow microporosity. Fast pyrolysis seems to hamper the porosity development, probably due to the suppression of decomposition reactions of functional groups and rearrangement of the carbonaceous matrix of the solid when pyrolysis takes place at fast heating rate.

In the case of acid treated biomass, different results are attained, and the porosity is vigorously developed. The micropore volume values obtained from N_2 and CO_2 adsorption isotherms, with $V_{DR}^{N2} > V_{DR}^{CO2}$, indicate the presence of wide microporosity in these solids (sizes larger than 0.7 nm) [80]. In terms of surface area (A_{BET}) and total pore volume ($V_{0.99}$), the porosity development of the solid fractions follows the sequence: PSC > OPC > SPC, probably, due to the presence of higher cellulose in PS [81–83]. Higher surface areas in activated carbons produced from cellulose than those of Kraft lignin are already reported in the work of Bedia et al. [82], which showed that the raw materials can have an enormous impact on porosity development. The A_{BET} value obtained for PSC solids with 1640 m^2/g, is comparable to those activated carbons obtained by chemical activation of hemp resides or pine dust with H_3PO_4, and much higher than those attained by H_3PO_4 treatment of lignin or cellulose alone [44,84]. The total pore volume of PSC is also the highest one, equal to 1.41 cm^3/g. In addition, $V_{meso}/V_{0.99}$ ratios of 0.701, 0.631, and 0.542 are obtained for OPC, PSC, and SPC solids, pointing out that the use of orange peel as raw material delivers wider mean porosity. This trend is confirmed by the average pore volume as estimated by $4{\cdot}V_T/A_{BET}$, being 4.5 nm for OPC vs 3.4 and 3.2 nm for PSC and SPC, respectively. However, when the pore size distribution is analyzed in detail, more differences arise. The NLDFT pore size distribution of the solid fractions from acid treated biomass pyrolysis is plotted in Fig. 6. Two common features are found in the PSDs of all the materials, namely i) narrow distribution of micropores (2 <nm) showing a maximum at 0.6 nm ii) broad distribution of mesopores running up to 20 nm. The position and extension of the PSD in the mesopore region are different. In the case of SPC solid, the mesopore size distribution ends at 10 nm and it does not show a distinctive maximum, pointing out the presence of narrow mesoporosity. PSC distribution of mesopores is centered at 2.6 nm, while OPC shows the broadest mesopore size distribution, with a maximum at 4.7 nm.

The generation of porosity can be related to the chemical reactions between H_3PO_4 and carbon precursors. The presence of C–O–PO_3 surface groups on some porous carbons prepared by chemical activation of biomass residues with H_3PO_4 at different temperatures was confirmed by XPS analyses [42,79,80]. These phosphates and/or polyphosphates groups seems to be responsible for the dilation process during activation [47], and they have a significant impact not only on the porous texture but on the surface chemistry of activated carbons, providing surface acidity [85], oxidation [86], and electrooxidation [87] resistance. Thus, the combination of a large surface area with the presence of mesopores and phosphorus groups make OPC and PSC solid fractions great candidates for their use as catalytic support and adsorbents in pollutant remediation [82,85,88–90]. In this sense, Valero-Romero et al. prepared phosphorus-containing mesoporous carbon from H3PO4 activation with olive stone that was successfully used as catalysts for methanol dehydration [88]. Additionally, H_3PO_4 modified biochar has been applied for removing toxic Cr (VI) by Nawaz et al. The results showed that chemically modified biochar developed a moderate amount of surface area (246 m^2g^{-1}) along with microporosity, showing Cr (VI) removal of 99.97% under optimized conditions [89]. In another study about the remediation of emergent pollutants, such as bisphenol A and carbamazepine, the use of a H_3PO_4-treated biochar showed a clear increase in the adsorption capacities [90].

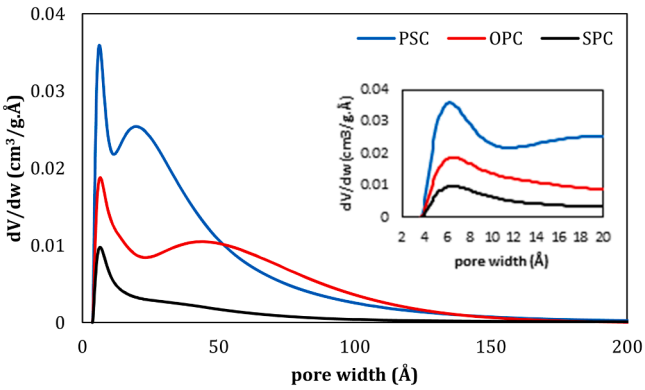

Fig. 6. Pore distribution of the solid residues obtained from acid treated biomass pyrolysis. Inset: micropore region.

Table 4
Characteristic parameters of the porous texture for solid residues under different pyrolysis conditions.

Sample	A_{BET} m^2 g^{-1}	V_{DR}^{N2} cm^3 g^{-1}	V_{meso} cm^3 g^{-1}	$V_{0.99}$ cm^3 g^{-1}	V_{DR}^{CO2} cm^3 g^{-1}
PSC	1640	0.52	0.89	1.42	0.26
OPC	870	0.29	0.68	0.97	0.16
SPC	300	0.11	0.13	0.25	0.07
PS (slow)	1.1	< 0.01	< 0.01	< 0.01	0.19
OP (slow)	1.0	< 0.01	< 0.01	0.01	0.11
SP (slow)	0.6	< 0.01	< 0.01	< 0.01	0.11
PS (fast)	1.0	< 0.01	< 0.01	< 0.01	0.08
OP (fast)	0.9	< 0.01	< 0.01	< 0.01	0.08
SP (fast)	0.9	< 0.01	< 0.01	< 0.01	0.07

4. Conclusions

The results obtained from the fixed-bed pyrolysis of pistachio shells, bitter orange peels and saffron petals under slow heating rate, fast heating rate and H_3PO_4 treatment conditions are herein reported.

Gas fraction of the fast pyrolysis is rich in C_2-C_3, CH_4 and H_2, increasing HHV. The H_3PO_4 treatment of biomasses leads to the evolution of higher syngas (CO and H_2), which also increases the HHV compared to slow pyrolysis. The composition of the gas fraction is affected by the presence of hemicellulose, pectins and inorganic matter in the feedstocks, which render a higher formation of CO_2, decreasing the HHV.

GC-MS results shows that the bio-oil obtained under fast and slow pyrolysis are richer in phenolic and acidic functional groups. However, fast pyrolysis promotes the formation of water, phenols, and ketones, while hindering the generation of N-compounds, carbohydrates and derivatives, acid, and furan compounds in the bio-oil. The bio-oil obtained from acid treated-biomass pyrolysis shows water as the main compound, with acids and aromatic compounds as the main components of the organic fraction.

Likewise, the HHV values of the solid residues obtained from fast pyrolysis are higher than those of slow pyrolysis. Acid catalyzed pyrolysis further enhances the HHVs. Additionally, among the biomasses, the PS solid residues show the highest HHVs, which is mostly related to the presence of lower inorganic matter. Moreover, SP and OP solid residues

present certain amounts of nitrogen in their composition, which could be valuable for the preparation of nitrogen-doped activated carbons. Solid residues obtained from acid treated biomass pyrolysis develop the porosity, being comparable to the values of apparent surface area of commercial activated carbons. The maximum porosity was achieved for PSC solid residue, with A_{BET} of 1640 m^2/g together with a total pore volume of 1.42 cm^3/g.

CRediT authorship contribution statement

Behnam Hosseinzaei: Methodology, Investigation, Visualization, Writing – original draft. **Mohammad Jafar Hadianfard:** Conceptualization, Validation, Supervision. **Ramiro Ruiz-Rosas:** Investigation, Visualization, Formal analysis, Data curation, Writing – review & editing. **Juana M. Rosas:** Data curation, Writing – review & editing. **José Rodríguez-Mirasol:** Conceptualization, Supervision, Project administration, Funding acquisition. **Tomás Cordero:** Conceptualization, Supervision, Project administration, Funding acquisition.

Declaration of Competing Interest

The authors declare that they have no known competing financial interests or personal relationships that could have appeared to influence the work reported in this paper.

Data availability

Data will be made available on request.

Acknowledgments

RRR, JMR, JRM and TC thank MICINN (RTI2018-097555-B-100) and Junta de Andalucía (P18-RT-4592) for financial support. Funding for open access charge: Universidad de Málaga/CBUA.

Appendix A. Supplementary material

Supplementary data associated with this article can be found in the online version at doi:10.1016/j.jaap.2022.105724.

References

[1] H.L. Chum, R.P. Overend, Biomass and renewable fuels, Fuel Process. Technol. 71 (1–3) (2001) 187–195, https://doi.org/10.1016/S0378-3820(01)00146-1.
[2] Y. Liao, S. Koelewijn, G. van den Bossche, J. Gvan Aelst, S. van den Bosch, T. Renders, K. Navare, T. Nicolaï, K. van Aelst, M. Maesen, H. Matsushima, J. Thevelein, K. van Acker, B. Lagrain, D. Verboekend, B. Sels, A sustainable wood biorefinery for low-carbon footprint chemicals production, Science 367 (6484) (2020) 1385–1390, https://doi.org/10.1126/science.aau1567.
[3] A. Mlonka-Mędrala, P. Evangelopoulos, M. Sieradzka, M. Zajemska, A. Magdziarz, Pyrolysis of agricultural waste biomass towards production of gas fuel and high-quality char: experimental and numerical investigations, Fuel 296 (2021), https://doi.org/10.1016/j.fuel.2021.120611.
[4] A. Taghizadeh-Alisaraei, H.A. Assar, B. Ghobadian, A. Motevali, Potential of biofuel production from pistachio waste in Iran, Renew. Sustain. Energy Rev. 72 (2017) 510–522, https://doi.org/10.1016/J.RSER.2017.01.111.
[5] IndexBox: Volume of World Pistachio Market in 2019 Grew By 4%, EastFruit. ⟨https://east-fruit.com/en/horticulture-market/market-reviews/indexbox-volume-of-world-pistachio-market-in-2019-grew-by-4/⟩, (Accessed 24 June 2022).
[6] L. Navarro, The Spanish citrus industry, Acta Hortic. (2015) 41–48, https://doi.org/10.17660/ActaHortic.2015.1065.1.
[7] Food and Agriculture Organization of the United Nations. ⟨https://www.fao.org/faostat/en/#home⟩, (Accessed 21 June 2022).
[8] Saffron Production in 2019, Alipour Inc. (n.d.). ⟨https://alipourinc.com/saffron-production-in-2019/⟩, (Accessed 1 February 2022).
[9] F.X. Collard, J. Blin, A review on pyrolysis of biomass constituents: Mechanisms and composition of the products obtained from the conversion of cellulose, hemicelluloses and lignin, Renew. Sustain. Energy Rev. 38 (2014) 594–608, https://doi.org/10.1016/J.RSER.2014.06.013.
[10] T.Y.A. Fahmy, Y. Fahmy, F. Mobarak, M. El-Sakhawy, R.E. Abou-Zeid, Biomass pyrolysis: past, present, and future, Environ. Dev. Sustain. 22 (1) (2020) 17–32, https://doi.org/10.1007/s10668-018-0200-5.
[11] S. Yaman, Pyrolysis of biomass to produce fuels and chemical feedstocks, Energy Convers. Manag. 45 (5) (2004) 651–671, https://doi.org/10.1016/S0196-8904(03)00177-8.
[12] S. Fiore, F. Berruti, C. Briens, Investigation of innovative and conventional pyrolysis of ligneous and herbaceous biomasses for biochar production, Biomass Bioenergy 119 (2018) 381–391, https://doi.org/10.1016/J.BIOMBIOE.2018.10.010.
[13] E. Fernandez, L. Santamaria, M. Amutio, M. Artetxe, A. Arregi, G. Lopez, J. Bilbao, M. Olazar, Role of temperature in the biomass steam pyrolysis in a conical spouted bed reactor, Energy 238 (2022), 122053, https://doi.org/10.1016/j.energy.2021.122053.
[14] J.L. Toro-Trochez, D.A. De Haro Del Río, L. Sandoval-Rangel, D. Bustos-Martínez, F.J. García-Mateos, R. Ruiz-Rosas, J. Rodríguez-Mirasol, T. Cordero, E.S. Carrilo-Pedraza, Catalytic fast pyrolysis of soybean hulls: focus on the products, J. Anal. Appl. Pyrolysis (2022) 163, https://doi.org/10.1016/j.jaap.2022.105492.
[15] D. Mohan, C.U. Pittman, P.H. Steele, Pyrolysis of wood/biomass for bio-oil: a critical review, Energy Fuels 21 (2006) 848–889, https://doi.org/10.1021/ef0502397.
[16] A. Pattiya, Bio-oil production via fast pyrolysis of biomass residues from cassava plants in a fluidised-bed reactor, Bioresour. Technol. 102 (2) (2011) 1959–1967, https://doi.org/10.1016/j.biortech.2010.08.117.
[17] R.M. Taib, N. Abdullah, N.S.M. Aziz, Bio-oil derived from banana pseudo-stem via fast pyrolysis process, Biomass Bioenergy 148 (2021), 106034, https://doi.org/10.1016/J.BIOMBIOE.2021.106034.
[18] G. Duman, C. Okutucu, S. Ucar, R. Stahl, J. Yanik, The slow and fast pyrolysis of cherry seed, Bioresour. Technol. 102 (2) (2011) 1869–1878, https://doi.org/10.1016/J.BIORTECH.2010.07.051.
[19] Z. Yang, A. Kumar, R.L. Huhnke, M. Buser, S. Capareda, Pyrolysis of eastern redcedar: distribution and characteristics of fast and slow pyrolysis products, Fuel 166 (2016) 157–165, https://doi.org/10.1016/J.FUEL.2015.10.101.
[20] R. Verma, S. Verma, S. Verma, J. Wang, J. Liu, B. Jing, K. Rakesh, Value-addition of wheat straw through acid treatment and pyrolysis of acid treated residues, J. Clean. Prod. 282 (2021), 124488, https://doi.org/10.1016/J.JCLEPRO.2020.124488.
[21] H. Wang, R. Srinivasan, F. Yu, P. Steele, Q. Li, B. Mitchell, A. Samala, Effect of acid, steam explosion, and size reduction pretreatments on bio-oil production from sweetgum, switchgrass, and corn stover, Appl. Biochem. Biotechnol. 167 (2012), https://doi.org/10.1007/s12010-012-9678-8.
[22] Z.L.L. Cueva, G.J. Griffin, L.P. Ward, S. Madapusi, K.V. Shah, R. Parthasarathy, A study of chemical pre-treatment and pyrolysis operating conditions to enhance biochar production from rice straw, J. Anal. Appl. Pyrolysis 163 (2022), 105455, https://doi.org/10.1016/j.jaap.2022.105455.
[23] T. Yang, A.C. Lua, Textural and chemical properties of zinc chloride activated carbons prepared from pistachio-nut shells, Mater. Chem. Phys. 100 (2–3) (2006) 438–444, https://doi.org/10.1016/J.MATCHEMPHYS.2006.01.039.
[24] B.S. Girgis, A.N.A. El-Hendawy, Porosity development in activated carbons obtained from date pits under chemical activation with phosphoric acid, Microporous Mesoporous Mater. 52 (2) (2002) 105–117, https://doi.org/10.1016/S1387-1811(01)00481-4.
[25] D. Prahas, Y. Kartika, N. Indraswati, S. Ismadji, Activated carbon from jackfruit peel waste by H3PO4 chemical activation: pore structure and surface chemistry characterization, Chem. Eng. J. 140 (1–3) (2008) 32–42, https://doi.org/10.1016/J.CEJ.2007.08.032.
[26] J.M. Rosas, J. Bedia, J. Rodríguez-Mirasol, T. Cordero, On the preparation and characterization of chars and activated carbons from orange skin, Fuel Process. Technol. 91 (10) (2010) 1345–1354, https://doi.org/10.1016/J.FUPROC.2010.05.006.
[27] P.B. Saynik, V.S. Moholkar, Insight into chemical pretreatment of hardwood (Arundo donax) for improvement of pyrolysis, Bioresour. Technol. Rep. (2020), 100545, https://doi.org/10.1016/j.biteb.2020.100545.
[28] S. Gupta, G.K. Gupta, M.K. Mondal, Slow pyrolysis of chemically treated walnut shell for valuable products: effect of process parameters and in-depth product analysis, Energy 181 (2019) 665–676, https://doi.org/10.1016/j.energy.2019.05.214.
[29] B. Hosseinzaei, M.J. Hadianfard, B. Aghabarari, M. García-Rollán, R. Ruiz-Rosas, J. M. Rosas, J. Rodríguez-Mirasol, T. Cordero, Pyrolysis of Pistachio Shell, Orange Peel and Saffron Petals for Bioenergy Production, Bioresour. Technol. Rep. 19 (2022) 101209, https://doi.org/10.1016/j.biteb.2022.101209.
[30] N.K. Fahim, S. Sadat, F. Janati, J. Feizy, Chemical composition of agriproduct saffron (Crocus sativus L.) petals and its safran (Crocus sativus), GIDA 37 (2012) 197–201.
[31] S. Gupta, G.K. Gupta, M.K. Mondal, Thermal degradation characteristics, kinetics, thermodynamic, and reaction mechanism analysis of pistachio shell pyrolysis for its bioenergy potential, Biomass Convers. Biorefin. (2020), https://doi.org/10.1007/s13399-020-01104-2.
[32] B.S. Kim, Y.M. Kim, J. Jae, J.C. Watanabe, S. Kim, S.C. Jung, S.C. Kim, Y.K. Park, Pyrolysis and catalytic upgrading of Citrus unshiu peel, Bioresour. Technol. 194 (2015) 312–319, https://doi.org/10.1016/j.biortech.2015.07.035.
[33] J.M. Rosas, J. Rodríguez-Mirasol, T. Cordero, NO reduction on carbon-supported chromium catalysts, Energy Fuels 24 (6) (2010) 3321–3328, https://doi.org/10.1021/ef901455v.
[34] ASTM E1131-08, Standard Test Method for Compositional Analysis by Thermogravimetry. ⟨https://webstore.ansi.org/standards/astm/astme113108⟩, (Accessed 8 February 2022).
[35] H. Yang, R. Yan, H. Chen, D.H. Lee, D.T. Liang, C. Zheng, Pyrolysis of palm oil wastes for enhanced production of hydrogen rich gases, Fuel Process. Technol. 87 (10) (2006) 935–942, https://doi.org/10.1016/J.FUPROC.2006.07.001.

[36] T. Cordero, F. Marquez, J. Rodriguez-Mirasol, J. Rodriguez, Predicting heating values of lignocellulosics and carbonaceous materials from proximate analysis, Fuel 80 (11) (2001) 1567–1571, https://doi.org/10.1016/S0016-2361(01)00034-5.
[37] M. Thommes, K. Kaneko, A. Neimark, J. Olivier, F. Rodriguez-Reinoso, J. Rouquerol, K. Sing, Physisorption of gases, with special reference to the evaluation of surface area and pore size distribution (IUPAC technical report), Pure Appl. Chem. 87 (9–10) (2015) 1051–1069, https://doi.org/10.1515/pac-2014-1117.
[38] A.E. Pütün, N. Özbay, E.A. Varol, B.B. Uzun, F. Ates, Rapid and slow pyrolysis of pistachio shell: effect of pyrolysis conditions on the product yields and characterization of the liquid product, Int. J. Energy Res. 31 (2007) 506–514, https://doi.org/10.1002/er.1263.
[39] J. Alvarez, B. Hooshdaran, M. Cortazar, M. Amutio, G. Lopez, F. Freire, M. Haghshenasfard, S. Hosseini, M. Olazar, Valorization of citrus wastes by fast pyrolysis in a conical spouted bed reactor, Fuel 224 (2018) 111–120, https://doi.org/10.1016/J.FUEL.2018.03.028.
[40] L. Aguiar, F. Márquez-Montesinos, A. Gonzalo, J.L. Sánchez, J. Arauzo, Influence of temperature and particle size on the fixed bed pyrolysis of orange peel residues, J. Anal. Appl. Pyrolysis 83 (1) (2008) 124–130, https://doi.org/10.1016/J.JAAP.2008.06.009.A.
[41] Sriram, G. Swaminathan, Pyrolysis of Musa balbisiana flower petal using thermogravimetric studies, Bioresour. Technol. 265 (2018) 236–246, https://doi.org/10.1016/j.biortech.2018.05.043.R.K.
[42] R.K. Sharma, J.B. Wooten, V.L. Baliga, M.R. Hajaligol, Characterization of chars from biomass-derived materials: Pectin chars, Fuel 80 (12) (2001) 1825–1836, https://doi.org/10.1016/S0016-2361(01)00066-7.
[43] O. Senneca, F. Cerciello, C. Russo, A. Wütscher, M. Muhler, B. Apicella, Thermal treatment of lignin, cellulose and hemicellulose in nitrogen and carbon dioxide, Fuel 271 (2020), 117656, https://doi.org/10.1016/J.FUEL.2020.117656.
[44] J.M. Rosas, J. Bedia, J. Rodríguez-Mirasol, T. Cordero, HEMP-derived activated carbon fibers by chemical activation with phosphoric acid, Fuel 88 (1) (2009) 19–26, https://doi.org/10.1016/J.FUEL.2008.08.004.
[45] F. Marquez-Montesinos, T. Cordero, J. Rodríguez-Mirasol, J.J. Rodríguez, CO_2 and steam gasification of a grapefruit skin char, 4, Fuel 81 (4) (2002) 423–429, https://doi.org/10.1016/S0016-2361(01)00174-0.
[46] D.J. Nowakowski, J.M. Jones, Uncatalysed and potassium-catalysed pyrolysis of the cell-wall constituents of biomass and their model compounds, J. Anal. Appl. Pyrolysis 83 (1) (2008) 12–25, https://doi.org/10.1016/j.jaap.2008.05.007.
[47] M. Jagtoyen, F. Derbyshire, Activated carbons from yellow poplar and white oak by H3PO4 activation, Carbon 36 (7–8) (1998) 1085–1097, https://doi.org/10.1016/S0008-6223(98)00082-7.
[48] V. Fierro, V. Torné-Fernández, A. Celzard, D. Montané, Influence of the demineralisation on the chemical activation of Kraft lignin with orthophosphoric acid, J. Hazard. Mater. 149 (1) (2007) 126–133, https://doi.org/10.1016/J.JHAZMAT.2007.03.056.
[49] I. Moulefera, F.J. García-Mateos, A. Benyoucef, J.M. Rosas, J. Rodríguez-Mirasol, T. Cordero, Effect of co-solution of carbon precursor and activating agent on the textural properties of highly porous activated carbon obtained by chemical activation of lignin with H3PO4, Front. Mater. 7 (2020), https://doi.org/10.3389/fmats.2020.00153.
[50] P. Álvarez, R. Santamaría, C. Blanco, M. Granda, Thermal degradation of lignocellulosic materials treated with several acids, J. Anal. Appl. Pyrolysis 74 (1–2) (2005) 337–343, https://doi.org/10.1016/J.JAAP.2004.11.030.
[51] J. Aburto, M. Moran, A. Galano, E. Torres-García, Non-isothermal pyrolysis of pectin: a thermochemical and kinetic approach, J. Anal. Appl. Pyrolysis 112 (2015) 94–104, https://doi.org/10.1016/J.JAAP.2015.02.012.
[52] Y. Le Brech, L. Jia, S. Cissé, G. Mauviel, N. Brosse, A. Dufour, Mechanisms of biomass pyrolysis studied by combining a fixed bed reactor with advanced gas analysis, J. Anal. Appl. Pyrolysis 117 (2016) 334–346, https://doi.org/10.1016/j.jaap.2015.10.013.
[53] J. Toro-Trochez, E. Carrillo-Pedraza, D. Bustos-Martínez, F. García-Mateos, R. Ruiz-Rosas, J. Rodríguez-Mirasol, T. Cordero, Thermogravimetric characterization and pyrolysis of soybean hulls, Bioresour. Technol. Rep. 6 (2019) 183–189, https://doi.org/10.1016/J.BITEB.2019.02.009.
[54] S. Al Arni, Comparison of slow and fast pyrolysis for converting biomass into fuel, Renew. Energy 124 (2018) 197–201, https://doi.org/10.1016/J.RENENE.2017.04.060.
[55] B.B. Uzun, A.E. Pütün, E. Pütün, Composition of products obtained via fast pyrolysis of olive-oil residue: effect of pyrolysis temperature, J. Anal. Appl. Pyrolysis 79 (1–2) (2007) 147–153, https://doi.org/10.1016/J.JAAP.2006.12.005.
[56] C. Setter, F.T.M. Silva, M.R. Assis, C.H. Ataíde, P.F. Trugilho, T.J.P. Oliveira, Slow pyrolysis of coffee husk briquettes: characterization of the solid and liquid fractions, Fuel 261 (2020), 116420, https://doi.org/10.1016/J.FUEL.2019.116420.
[57] I. Torri, V. Paasikallio, C. Faccini, R. Huff, E. Caramão, V. Sacon, A. Oasmaa, C. Zini, Bio-oil production of softwood and hardwood forest industry residues through fast and intermediate pyrolysis and its chromatographic characterization, Bioresour. Technol. 200 (2016) 680–690, https://doi.org/10.1016/J.BIORTECH.2015.10.086.
[58] P.J. de Wild, W.J.J. Huijgen, R.J.A. Gosselink, Lignin pyrolysis for profitable lignocellulosic biorefineries, Biofuels Bioprod. Biorefin. 8 (5) (2014) 645–657, https://doi.org/10.1002/bbb.1474.
[59] K. Zeka, K.C. Ruparelia, M.A. Continenza, D. Stagos, F. Vegliò, R.R.J. Arroo, Petals of Crocus sativus L. as a potential source of the antioxidants crocin and kaempferol, Fitoterapia 107 (2015) 128–134, https://doi.org/10.1016/j.fitote.2015.05.014.
[60] X.M. Chen, A.R. Tait, D.D. Kitts, Flavonoid composition of orange peel and its association with antioxidant and anti-inflammatory activities, Food Chem. 218 (2017) 15–21, https://doi.org/10.1016/j.foodchem.2016.09.016.
[61] G. Chang, P. Miao, X. Yan, G. Wang, Q. Guo, Phenol preparation from catalytic pyrolysis of palm kernel shell at low temperatures, Bioresour. Technol. 253 (2018) 214–219, https://doi.org/10.1016/J.BIORTECH.2017.12.084.
[62] J. Alvarez, G. Lopez, M. Amutio, J. Bilbao, M. Olazar, Bio-oil production from rice husk fast pyrolysis in a conical spouted bed reactor, Fuel 128 (2014) 162–169, https://doi.org/10.1016/J.FUEL.2014.02.074.
[63] S.C. Moldoveanu, Analytical Pyrolysis of Polymeric Carbohydrates, 2021. ⟨DOI: 10.1016/b978-0-12-818571-1.00004-2⟩.
[64] C. Branca, P. Giudicianni, C. di Blasi, GC/MS characterization of liquids generated from low-temperature pyrolysis of wood, Ind. Eng. Chem. Res. 42 (14) (2003) 3190–3202, https://doi.org/10.1021/ie030066d.
[65] J.S. Kim, G.G. Choi, Pyrolysis of lignocellulosic biomass for biochemical production. Waste Biorefinery: Potential and Perspectives, 2018, pp. 323–348, https://doi.org/10.1016/B978-0-444-63992-9.00011-2.
[66] S.D. Stefanidis, K.G. Kalogiannis, E.F. Iliopoulou, C.M. Michailof, P.A. Pilavachi, A. A. Lappas, A study of lignocellulosic biomass pyrolysis via the pyrolysis of cellulose, hemicellulose and lignin, J. Anal. Appl. Pyrolysis 105 (2014) 143–150, https://doi.org/10.1016/J.JAAP.2013.10.013.
[67] H. Ito, The formation of maltol and isomaltol through degradation of sucrose, Agric. Biol. Chem. 41 (7) (1997) 1307–1308, https://doi.org/10.1080/00021369.1977.10862669.
[68] H. Chen, Y. Xie, W. Chen, M. Xia, K. Li, Z. Chen, Y. Chen, H. Yang, Investigation on co-pyrolysis of lignocellulosic biomass and amino acids using TG-FTIR and Py-GC/MS, Energy Convers. Manag. 196 (2019) 320–329, https://doi.org/10.1016/j.enconman.2019.06.010.
[69] S.M. Jadouali, H. Atifi, R. Mamouni, K. Majourhat, Z. Bouzoubaâ, A. Laknifli, A. Faouzi, Chemical characterization and antioxidant compounds of flower parts of Moroccan Crocus sativus L. J. Saudi Soc. Agric. Sci. 18 (4) (2019) 476–480, https://doi.org/10.1016/j.jssas.2018.03.007.
[70] Q. Wang, H. Song, S. Pan, N. Dong, X. Wang, S. Sun, Initial pyrolysis mechanism and product formation of cellulose: an experimental and density functional theory (DFT) study, Sci. Rep. 10 (1) (2020) 1–18, https://doi.org/10.1038/s41598-020-60095-2.
[71] M. Amutio, G. Lopez, J. Alvarez, M. Olazar, J. Bilbao, Fast pyrolysis of eucalyptus waste in a conical spouted bed reactor, Bioresour. Technol. 194 (2015) 225–232, https://doi.org/10.1016/J.BIORTECH.2015.07.030.
[72] M.J. Mostazo-López, R. Ruiz-Rosas, E. Morallón, D. Cazorla-Amorós, Generation of nitrogen functionalities on activated carbons by amidation reactions and Hofmann rearrangement: chemical and electrochemical characterization, Carbon 91 (2015) 252–265, https://doi.org/10.1016/j.carbon.2015.04.089.
[73] M.J. Mostazo-López, D. Salinas-Torres, R. Ruiz-Rosas, E. Morallón, D. Cazorla-Amorós, Nitrogen-doped superporous activated carbons as electrocatalysts for the oxygen reduction reaction, Materials 12 (8) (2019) 2–17, https://doi.org/10.3390/ma12081346.
[74] T. Cordero-Lanzac, J. Rodríguez-Mirasol, T. Cordero, J. Bilbao, Advances and challenges in the valorization of bio-oil: hydrodeoxygenation using carbon-supported catalysts, Energy Fuels 35 (21) (2021) 17008–17031, https://doi.org/10.1021/acs.energyfuels.1c01700.
[75] M.L. Nieva Lobos, P. Campitelli, M.A. Volpe, E.L. Moyano, Catalytic and non-catalytic pyrolysis of Kraft pulp waste into anhydrosugars containing bio-oils and non-phytotoxic biochars, J. Anal. Appl. Pyrolysis 122 (2016) 216–223, https://doi.org/10.1016/J.JAAP.2016.09.021.
[76] J. Wu, W. Chen, L. Chen, X. Jiang, Super-high N-doping promoted formation of sulfur radicals for continuous catalytic oxidation of H2S over biomass derived activated carbon, J. Hazard. Mater. 424 (2022), 127648, https://doi.org/10.1016/J.JHAZMAT.2021.127648.
[77] D. Yao, Q. Hu, D. Wang, H. Yang, C. Wu, X. Wang, H. Chen, Hydrogen production from biomass gasification using biochar as a catalyst/support, Bioresour. Technol. 216 (2016) 159–164, https://doi.org/10.1016/J.BIORTECH.2016.05.011.
[78] B. Khiari, I. Ghouma, A.I. Ferjani, A.A. Azzaz, S. Jellali, L. Limousy, M. Jeguirim, "Kenaf stems: thermal characterization and conversion for biofuel and biochar production, Fuel vol. 262 (2020), 116654, https://doi.org/10.1016/j.fuel.2019.116654.
[79] K. Weber, P. Quicker, Properties of biochar, Fuel 217 (2018) 240–261, https://doi.org/10.1016/J.FUEL.2017.12.054.
[80] D. Lozano-Castelló, D. Cazorla-Amorós, A. Linares-Solano, Usefulness of CO_2 adsorption at 273 K for the characterization of porous carbons, Carbon 42 (7) (2004) 1233–1242, https://doi.org/10.1016/J.CARBON.2004.01.037.
[81] G. Chu, J. Zhao, Y. Huang, D. Zhou, Y. Liu, M. Wu, H. Peng, Q. Zhao, B. Pan, C. Steinberg, Phosphoric acid pretreatment enhances the specific surface areas of biochars by generation of micropores, Environ. Pollut. 240 (2018) 1–9, https://doi.org/10.1016/J.ENVPOL.2018.04.003.
[82] J. Bedia, J.M. Rosas, J. Márquez, J. Rodríguez-Mirasol, T. Cordero, Preparation and characterization of carbon based acid catalysts for the dehydration of 2-propanol, Carbon 47 (1) (2009) 286–294, https://doi.org/10.1016/J.CARBON.2008.10.008.
[83] R. Fu, L. Liu, W. Huang, P. Sun, Studies on the structure of activated carbon fibers activated by phosphoric acid, Appl. Polym. Sci. 87 (14) (2003) 2253–2261, https://doi.org/10.1002/app.11607.
[84] A.M. Puziy, O.I. Poddubnaya, A.M. Ziatdinov, On the chemical structure of phosphorus compounds in phosphoric acid-activated carbon, Appl. Surf. Sci. 252 (23) (2006) 8036–8038, https://doi.org/10.1016/J.APSUSC.2005.10.044.
[85] M.J. Valero-Romero, E. María Calvo-Muñoz, R. Ruiz-Rosas, J. Rodríguez-Mirasol, T. Cordero, Phosphorus-containing mesoporous carbon acid catalyst for methanol

dehydration to dimethyl ether, Ind. Eng. Chem. Res. 58 (10) (2019) 4042–4053, https://doi.org/10.1021/acs.iecr.8b05897.

[86] J.M. Rosas, R. Ruiz-Rosas, J. Rodríguez-Mirasol, T. Cordero, Kinetic study of the oxidation resistance of phosphorus-containing activated carbons, Carbon 50 (4) (2012) 1523–1537, https://doi.org/10.1016/J.CARBON.2011.11.030.

[87] R. Berenguer, R. Ruiz-Rosas, A. Gallardo, D. Cazorla-Amorós, E. Morallón, H. Nishihara, T. Kyotani, J. Rodríguez-Mirasol, T. Cordero, Enhanced electro-oxidation resistance of carbon electrodes induced by phosphorus surface groups, Carbon 95 (2015) 681–689, https://doi.org/10.1016/J.CARBON.2015.08.101.

[88] M.J. Valero-Romero, E.M. Calvo-Muñoz, R. Ruiz-Rosas, J. Rodríguez-Mirasol, T. Cordero, Phosphorus-containing mesoporous carbon acid catalyst for methanol dehydration to dimethyl ether, Ind. Eng. Chem. Res. 58 (2019) 4042–4053, https://doi.org/10.1021/acs.iecr.8b05897.

[89] A. Nawaz, B. Singh, P. Kumar, H3PO4-modified Lagerstroemia speciosa seed hull biochar for toxic Cr(VI) removal: isotherm, kinetics, and thermodynamic study, Biomass Convers. Biorefin. (2021), https://doi.org/10.1007/s13399-021-01780-8.

[90] G. Chu, J. Zhao, Y. Huang, D. Zhou, Y. Liu, M. Wu, H. Peng, Q. Zhao, B. Pan, C.E. W. Steinberg, Phosphoric acid pretreatment enhances the specific surface areas of biochars by generation of micropores, Environ. Pollut. 240 (2018) 1–9, https://doi.org/10.1016/j.envpol.2018.04.003.